0254-6124/2020/40(2)-207–08 *Chin. J. Space Sci.* 空间科学学报

DAI Yaru, PAN Weilin, QIAO Shuai, HU Xiong, YAN Zhaoai, BAN Chao. Seasonal variations of mesospheric densities observed by Rayleigh lidar at Golmud, Qinghai. *Chin. J. Space Sci.*, 2020, **40**(2): 207-214. DOI:10.11728/cjss2020.02.207

Seasonal Variations of Mesospheric Densities Observed by Rayleigh Lidar at Golmud, Qinghai*

DAI Yaru[1,2,3] PAN Weilin[2,3] QIAO Shuai[4]

HU Xiong[1] YAN Zhaoai[1,3] BAN Chao[2]

1(*Near-space Environment Laboratory, National Space Science Center, Chinese Academy of Sciences, Beijing* 100190)

2(*Key Laboratory of Middle Atmosphere and Global Environment Observation, Institute of Atmospheric Physics, Chinese Academy of Sciences, Beijing* 100029)

3(*University of Chinese Academy of Sciences, Beijing* 100049)

4(*Zhongneng Power-Tech Development Company of Limited, Beijing* 100034)

Abstract From Aug. 2013 to Oct. 2015, a Rayleigh lidar has been used to study the middle atmosphere at Golmud (36.25°N, 94.54°E), Qinghai, located in the northeastern part of the Tibetan Plateau. Mesospheric density profiles from 50 to 90 km were retrieved based on 205 nights of lidar observation, with a total of 1616 hours of operation. We compared our lidar density measurements with SABER observations onboard TIMED satellite and MSIS-00 model data. The results showed that the annual mean density measured by lidar agreed well with SABER data, but both were lower than that of MSIS-00. All datasets exhibited dominant annual oscillation in the mesosphere. From 63 to 85 km, the annual amplitude of lidar density is larger than those of SABER and MSIS-00. PDD (Percentage of Density Difference) was calculated to investigate the mesospheric density climatology. The largest density variations of lidar, MSIS-00, and SABER occurred at around 72 km. Both lidar and SABER PDD reached their maximum in May, about one month earlier than the MSIS-00; while the minimum PDD appeared in late December for all datasets.

Key words Lidar, SABER, MSIS model, Mesospheric density, Seasonal variations

Classified index P 351

0 Introduction

The dynamics and chemistry of the middle atmosphere are believed to have a close relationship with global climate change[1,2]. Mesosphere interacts with thermosphere, stratosphere, and troposphere through dynamical entities, such as tides, planetary waves, and gravity waves[3−6]. Estimation of the mesospheric density is also critical for low-Earth-orbit satellite operations, including orbit determination and reentry calculation.

Modeling studies have revealed the variations of atmospheric density in response to various atmospheric processes. MSIS is an empirical atmospheric model firstly developed by Hedin[7], and then widely used as a convenient tool for middle atmosphere study. Based on its latest version, the MSIS-00 model[8], Ling and Chen[9] simulated the atmospheric density and temperature variations from 50 to 140 km.

Middle atmosphere has been investigated by lidars, radars, and satellites[10−12]. Thermospheric density can be inferred from accelerometer mea-

* Supported by the National Key R and D Program of China (2018YFC1407301, 2016YFC1400301) and the National Natural Science Foundation of China (41127901)

Received February 25, 2019. Revised December 25, 2019

E-mail: panweilin@mail.iap.ac.cn

surements by satellites[13−16]. Neutral density below 30 km is regularly obtained from the radiosonde. Rockets occasionally make in-situ measurements of mesospheric density[17,18]. Meteor radar measurements were recently used to obtain relative density in the mesopause region[19].

SABER (Sounding of the Atmosphere using Broadband Emission Radiometry), one of the four instruments onboard NASA TIMED (Thermosphere Ionosphere Mesosphere Energetics Dynamics) satellite, has been used for making global measurements of the middle atmosphere[20,21]. Xiao *et al.*[22] used SABER data to characterize the atmospheric densities from 20 to 100 km.

For decades, lidars have been used to make atmospheric density observations[23−25]. Rayleigh lidar can obtain middle atmosphere density with high spatial and temporal resolutions. Hauchecorne and Chanin[23] measured the temperature and density from 30 to 90 km based on Rayleigh lidar at Haute station. In 1999, atmospheric density and temperature profiles of the middle and upper stratosphere were obtained in Hefei using dual-wavelength Rayleigh lidar[26].

Long-term observations of Rayleigh lidars have been used to analyze the seasonal variations of middle atmosphere density. Rayleigh lidar measurements at Utah State University from 1993 to 2004 were used to characterize the climatology of the relative density from 45 to 90 km[27].

In this paper, the lidar measurements of mesospheric density at Golmud are reported, and then compared with MSIS-00 model data and SABER observations.

1 Observations and Data Processing Method

1.1 Lidar Observations

A Rayleigh lidar, named MARMOT (Middle Atmosphere Remote Mobile Observatory in Tibet), was developed by the Institute of Atmospheric Physics, Chinese Academy of Sciences. From Aug. 2013 to Oct. 2015, it was deployed at the Golmud Meteorological Bureau (36.25°N, 94.54°E, 2808 m A.S.L.), located at the northeastern part of the Tibetan Plateau. The system was operated for more than three years to make atmospheric density, temperature, and aerosol measurements.

The MARMOT lidar consists of three components: a laser transmitter, an optical receiver, and a signal acquisition and control unit. A dual-telescope configuration can collect the Rayleigh backscatter signals separately from 30 to 60 km and from 50 to 90 km, in order to accommodate the large dynamic range of lidar signal[28]. In this paper, we only use the data between 50 and 90 km for mesospheric density study. The total observation lengths for each month during 2013 to 2015 are listed in Table 1, with a total of 1616 hours spanning in 205 days. The typical observation duration is about 8 hours per night, with a minimum of 2 hours per night.

1.2 Density Retrieval Method

In the Rayleigh scattering process, the molecular scattered lidar signal is proportional to the atmospheric density. After compensating for the range dependence, we can obtain atmospheric density profiles with the help of the absolute density value at a reference altitude. The equation is as follows:

$$\rho(z) = \frac{z^2\rho(z_0)[N(z) - B]}{z_0^2[N(z_0) - B]}, \tag{1}$$

where $\rho(z)$ is the atmospheric density at the altitude z, $N(z)$ is lidar received signal at the altitude z, B

Table 1 MARMOT observation lengths at Golmud (unit h)

	2013	2014	2015
Jan.	–	65	–
Feb.	–	–	–
Mar.	–	–	–
Apr.	–	–	79
May.	–	–	92
Jun.	–	12	–
Jul.	–	90	85
Aug.	18	93	71
Sept.	17	100	7
Oct.	62	179	131
Nov.	–	204	–
Dec.	83	228	–

is background noise, and z_0 is the reference altitude. In our case, we used the SABER satellite density data at 50 km as the reference to calculate the absolute density[29]. The vertical resolution of lidar density profile was set to be 300 m, and a 2 km (FWHM) Hamming window was applied for data smoothing.

The uncertainty of lidar density is mainly caused by the random statistical error of photons, which obeys the Poisson distribution. Therefore, the relative uncertainty of lidar density can be expressed as

$$\frac{\Delta\rho(z)}{\rho(z)} \approx \frac{\sqrt{N(z)}}{N(z)-B}. \tag{2}$$

Figure 1 shows a typical density profile and corresponding relative error. The lidar data was taken on 27 Dec. 2014, with an observation length of 12 hours.

As shown in Figure 1, atmospheric density decreases exponentially from $10^{-3}\,\mathrm{kg\cdot m^{-3}}$ at 50 km to $3\times10^{-6}\,\mathrm{kg\cdot m^{-3}}$ at 90 km, spanning about 3 orders of magnitude. The relative error of density increases with altitude, but within 2% in the altitude range from 50 to 90 km. To better illustrate the density variations, we calculated the PDD (Percentage of Density Difference) as follows:

$$\Delta\rho(z) = \frac{\rho(z)-\bar{\rho}(z)}{\bar{\rho}(z)}, \tag{3}$$

where $\bar{\rho}(z)$ is the annual mean density.

2 Seasonal Variations Analysis

2.1 Spectral Analysis of Mesospheric Density

To examine the mesospheric density climatology, we neglected any inter-annual variations within the three-year period from Aug. 2013 to Oct. 2015, and combined all data into a composite dataset. Firstly, nightly density profiles from 50 to 90 km were retrieved using Eq. (1). Then weekly mean profiles were calculated by taking the average on nightly profiles. Due to the fact that there were some weeks with no lidar observation data available, we obtained a total of 34 weekly mean profiles in a composite year of 52 weeks.

For the same time period from Aug. 2013 to Oct. 2015, we also obtained the nightly mesospheric density profiles from the MSIS-00 model and from SABER observations. The MSIS-00 model data was chosen to cover the same latitude and longitude at Golmud, while the SABER data to cover the area within ±5° latitude (31.25°−41.25°N) and ±10° longitude (84.54°−104.54°E) around the lidar site. Typically there are about 2∼4 SABER data profiles in one night. For both MSIS-00 and SABER, there were 52 weekly mean density profiles in a composite year.

Next, spectral analysis on the lidar, MSIS-00, and SABER data at Golmud are conducted. To examine the harmonic components of weekly mean me-

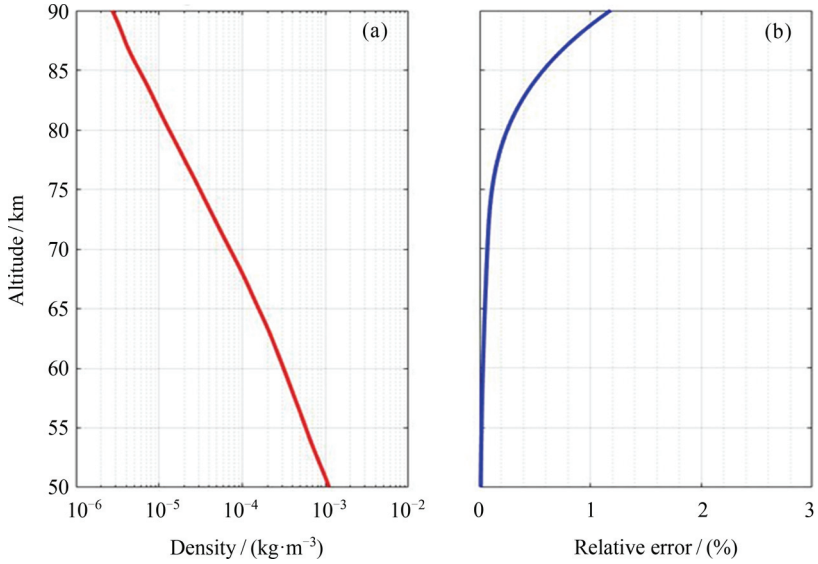


Fig. 1 Typical atmospheric density and relative error profiles based on lidar measurements on 27 Dec. 2014

sospheric density, the Lomb-Scargle periodogram was performed on each dataset[30]. Figure 2 shows the normalized power spectrums of lidar, MSIS-00 and SABER densities. In Figure 2 at each altitude from 50 to 90 km, normalized power spectrums that satisfying the 90% significance testing are plotted in color contour. The 52- and 26-week components of densities have been identified in the mesosphere, with a dominant annual oscillation peaking at around 70 km. A relatively weaker semiannual oscillation is also presented for each dataset.

2.2 Lidar Density Data Interpolation

As mentioned above, there were 34 weekly mean lidar density profiles in a composite year, with no lidar data in February and March, as shown in Table 1. In order to fill in the gaps of missing data, a nonlinear fitting method was applied for lidar data interpolation. We defined a nonlinear function with 52- and 26-week harmonic components as follows:

$$\rho_{\text{fit}} = A_0 + A_1 \cos\left[\frac{2\pi}{52}(n_{\text{wk}} - \varphi_1)\right] + A_2 \cos\left[\frac{2\pi}{26}(n_{\text{wk}} - \varphi_2)\right], \quad (4)$$

where ρ_{fit} is the weekly density, A_0 is the annual mean density, A_1 and A_2 are the amplitudes of 52- and 26-week components, respectively, φ_1 and φ_2 are their corresponding phases, and n_{wk} represents the week number.

Data fitting was conducted on the weekly densities of lidar, MSIS-00, and SABER. The fits were computed sequentially. An annual mean plus 52-week fit was firstly computed and then subtracted from the original dataset before the 26-week fit was computed[31]. Figure 3 shows the weekly densities in blue asterisk, with the fitting results plotted in red line at 50, 60, 70, and 80 km, respectively. It can be seen that this fitting method can reconstruct the missing lidar data reasonably well. At these altitudes, lidar and SABER data agree well with each other, but both are lower than MSIS-00.

2.3 Annual Mean Density

The fitting coefficient A_0, that is, the annual mean densities of lidar, MSIS-00, and SABER are plotted in Figure 4(a). They all decrease exponentially with altitude increasing. To illustrate their discrepancies, the density ratio of lidar to MSIS-00, and the ratio of SABER to MSIS-00 are shown in Figure 4(b), with the ratio value from 50 to 90 km varying between 0.82 and 0.96. We can see that the densities measured by lidar and SABER agreed well, with their differences within about 2%. The density measurements (for both lidar and SABER) are deviated from the MSIS-00 model by about 5% at 50 km and increasingly by about 16% at 90 km. The two red dashed lines in Figure 4(b) re-

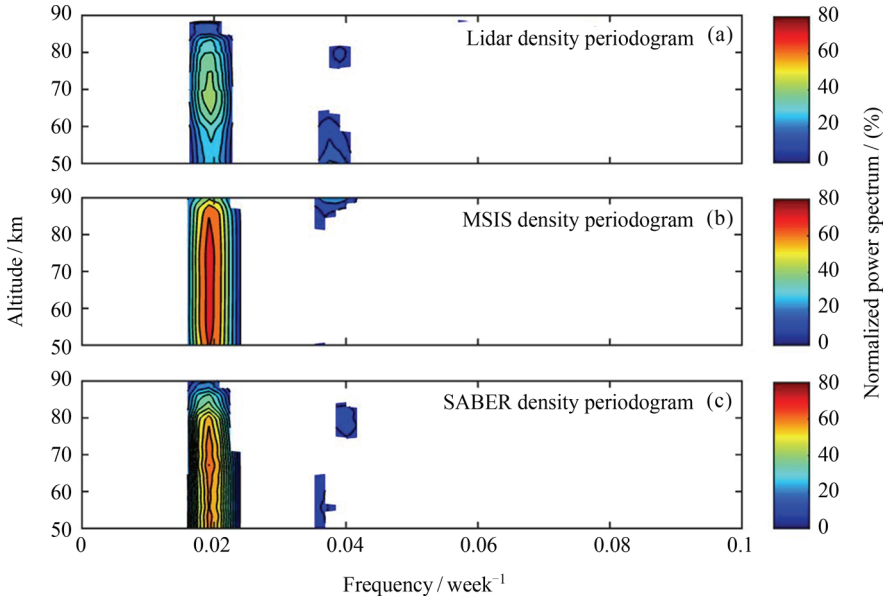


Fig. 2 Normalized power spectrums of lidar, MSIS-00, and SABER densities

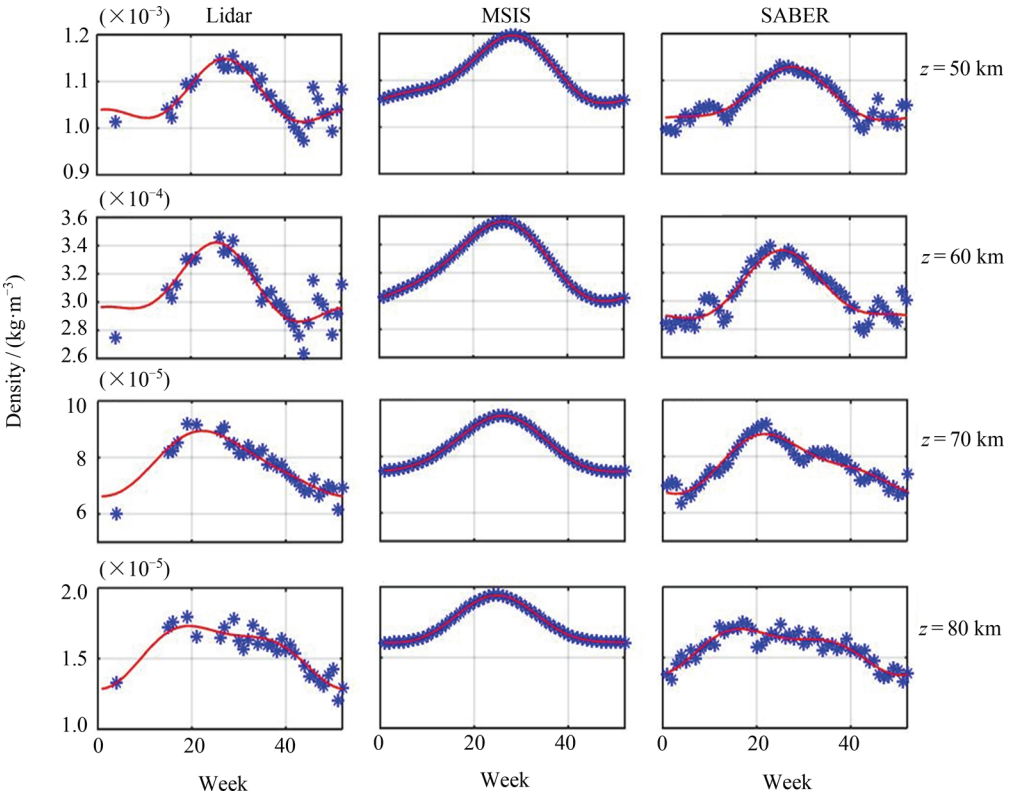


Fig. 3 Weekly data (in blue asterisk) and data fitting (in red line) of lidar, MSIS-00, and SABER densities at 50, 60, 70, and 80 km, respectively

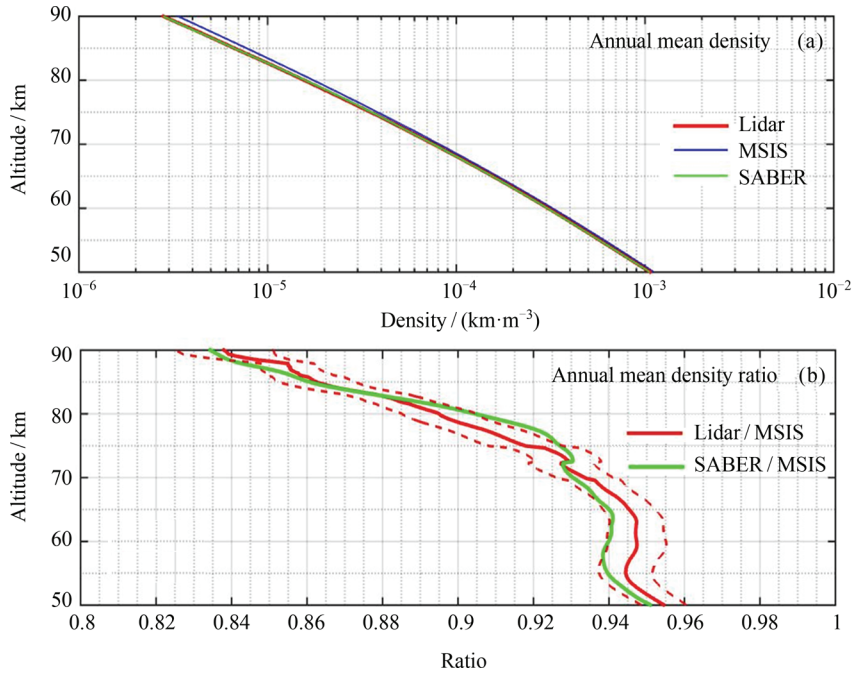


Fig. 4 Annual mean density profiles of lidar (in red line), MSIS-00 (in blue line) and SABER (in green line). The annual mean density ratios of SABER to MSIS-00 (in green line), and lidar to MSIS-00 (in red solid line) with lidar data fitting errors (in red dashed line)

present the standard errors by computing the estimated variance-covariance of lidar data fitting coefficient A_0. This uncertainty was induced by the nonlinear fitting method described in Section 2.2. It shows the uncertainty of lidar annual mean density within about 2% from 50 to 90 km.

2.4 Density Oscillation Components

The fitting parameters of annual and semiannual amplitudes (A_1 and A_2) can be used to characterize density oscillation strength. We calculated the ratio of annual amplitude to mean density, as well as the ratio of semiannual amplitude to mean. Figure 5 shows that annual components are mostly stronger than semiannual ones from 50 to 90 km. The annual oscillations vary from 2% to 16%, while the semiannual oscillations mostly within 5%. Between 63 and 85 km, the annual oscillation of lidar is stronger than both MSIS-00 and SABER, with a peak of about 16% for lidar around 74 km, while the strongest annual oscillation for both MSIS-00 and SABER are about 12% at around 73 km.

2.5 Seasonal Variation Comparisons

In order to characterize the mesospheric density climatology, we use Eq. (3) to calculate PDD from density data. The weekly PDD profiles of lidar, MSIS-00, and SABER are plotted in color contour in Figures 6 (a) (b) (d), respectively. The SABER data was processed using the same lidar data fitting method as described in Section 2.2, and the results are plotted in Figure 6(c).

It can be seen that seasonal variations of these four datasets were all dominated by annual oscillations. The PDD from 50 to 90 km is mostly positive in summer and negative in winter. The lidar and SABER PDD peak in late May with a value of 18% for lidar and 14% for SABER, both at around 72 km. The PDD of MSIS-00 reaches its maximum value of 14% at about the same altitude, but in late June, which is one month later than both lidar and SABER observations. This one-month lag of time between lidar and model is consistent with the previous study by Utah State University (USU) lidar group[27]. The PDD minimum of lidar, MSIS-00, and SABER are −20%, −14% and −14%, respectively, all appearing in late December. It is noticeable from the color contour plot in Figure 6 that both lidar and SABER observations show an asymmetric structure during the transitional periods in spring and autumn, while the MSIS-00 exhibits relatively symmetric transitions over the same period. It has been noticed that the highest and the lowest PDDs are both at around 72 km for all four datasets. The same phenomenon was also seen from

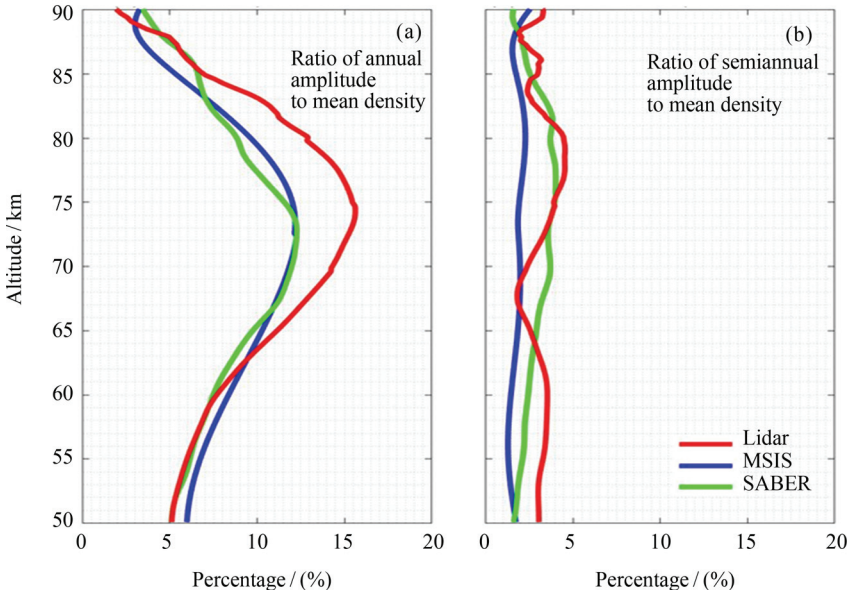


Fig. 5 Ratio of annual amplitude to mean density and the ratio of semiannual amplitude to mean density for lidar, MSIS-00, and SABER

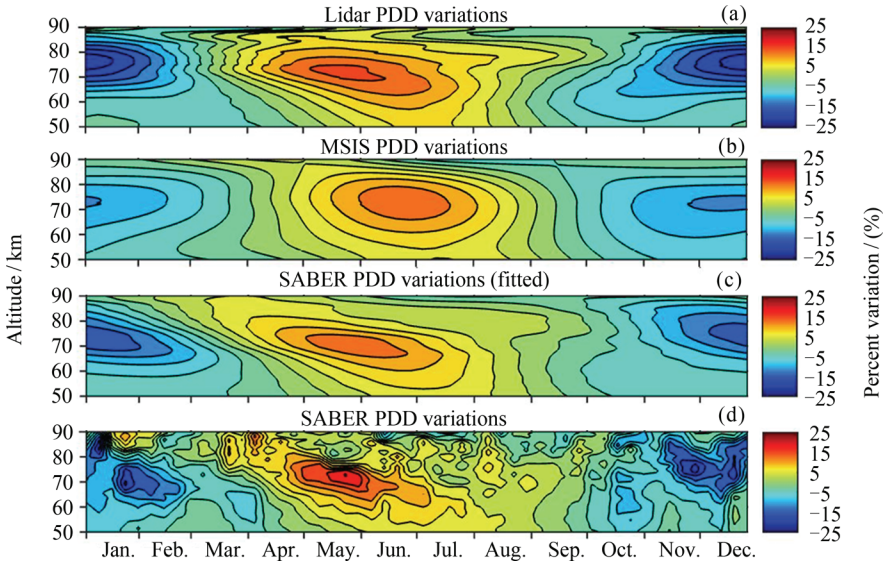


Fig. 6 Seasonal variations of PDD derived from lidar, MSIS-00, the SABER fitting data, and SABER observational data

the USU lidar results[27]. The underlying mechanism is yet fully understood for explaining this feature, but we speculate that it could be related to mesospheric dynamics influence. Further investigations are needed for conducting a more comprehensive study on this open question.

3 Summary

Ground-based Rayleigh lidar measurements from Aug. 2013 to Oct. 2015 were used to analyze the mesospheric density climatology from 50 to 90 km at Golmud. Spectral analysis showed that harmonic components of 52- and 26-week were presented in lidar, MSIS-00, and SABER density data. Therefore, for those weeks with no lidar observation available, a nonlinear fitting method has been used for data interpolation to fill in the gap. The annual mean density comparisons showed that lidar and SABER data agreed well with each other, but both are consistently lower than MSIS-00. Then PDDs were calculated for lidar, MSIS-00, SABER fitting data, and SABER observational data. Each dataset exhibits a dominating annual cycle, with positive variations in summer and negative in winter. Lidar and SABER observations revealed an asymmetric structure during the spring and fall transitional periods, compared to the symmetry exhibited in MSIS-00 model.

The inconsistencies between the observational datasets and the model may indicate some limitations of MSIS-00, which is an empirical atmospheric model based on observations acquired about two decades ago, especially over the Tibetan Plateau area, where mesospheric data is scarce. The model could be further improved by adding more observations into the database in the future.

Acknowledgements The authors would like to acknowledge the MARMOT lidar team for making the lidar measurements, the Golmud Meteorological Bureau for providing the observation site, the Naval Research Lab. (NRL) for providing the MSIS-00 model data, and the NASA TIMED team for providing the SABER data.

References

[1] LABITZKE K. Temperature changes in the mesosphere and stratosphere connected with circulation changes in winter [J]. *J. Atmos. Sci.*, 1972, **29**(4): 756-766

[2] ROBLE R G, DICKINSON R E. How will changes in carbon dioxide and methane modify the mean structure of the mesosphere and thermosphere [J]. *Geophys. Res. Lett.*, 1989, **16**: 1441-1444

[3] HOLTON J R. The influence of gravity wave breaking on the general circulation of the middle atmosphere [J]. *J. Atmos. Sci.*, 1983, **40**(10): 2497-2507

[4] LIU H L, ROBLE R G. A study of a self-generated stratospheric sudden warming and its mesospheric lower thermospheric impacts using the coupled TIME-

GCM/CCM3 [J]. *J. Geophys. Res.*, 2002, **107**(D23): 4695

[5] YUAN T, THURAIRAJAH B, SHE C Y, *et al.* Wind and temperature response of midlatitude mesopause region to the 2009 Sudden Stratospheric Warming [J]. *J. Geophys. Res.*, 2012, **117**: D09114

[6] SOX L, WICKWAR V, FISH C, *et al.* Temperature deviations in the midlatitude mesosphere during stratospheric warmings as measured with Rayleigh-scatter lidar [C]//The 27th International Laser Radar Conference. New York: the International Laser Radar Conference, 2015: 1441-1444

[7] HEDIN A E, SALAH J E, EVANS J V, *et al.* A global thermospheric model based on mass spectrometer and incoherent scatter data, MSIS 1. N_2 density and temperature [J]. *J. Geophys. Res.*, 1977, **82**: 2139-2147

[8] PICONE J M, HEDIN A E, DROB D P, *et al.* NRLMSISE-00 empirical model of the atmosphere: statistical comparisons and scientific issues [J]. *J. Geophys. Res.*, 2002, **107**(A12): 1468

[9] LING C, CHEN Z. Monthly averaged atmospheric conditions in the transition flow region of China based on the NRLMSISE-00 model [J]. *Spacecraft Environ. Eng.*, 2015, **32**(3): 236-242

[10] MCLRESS C, SHEPHERD G G, SOLHEIM B H, *et al.* Combined mesosphere/thermosphere winds using WINDII and HRDI data from the Upper Atmosphere Research Satellite [J]. *J. Geophys. Res.*, 1996, **1011**(D6): 10441-10454

[11] SHE C Y, CHEN S, HU Z, *et al.* Eight-year climatology of nocturnal temperature and sodium density in the mesopause region (80 to 105 km) over Fort Collins, Co (41°N, 105°W) [J]. *Geophys. Res. Lett.*, 2000, **27**(20): 3289-3292

[12] SIVAKUMAR V, PRASANTH P V, KISHORE P, *et al.* Rayleigh LIDAR and satellite (HALOE, SABER, CHAMP and COSMIC) measurements of stratosphere-mesosphere temperature over a southern sub-tropical site, Reunion (20.8°S; 55.5°E): climatology and comparison study [J]. *Ann. Geophys.*, 2011, **29**(4): 649-662

[13] BRUINSMA S, FORBES J M, NEREM R S, *et al.* Thermosphere density response to the 20—21 November 2003 solar and geomagnetic storm from CHAMP and GRACE accelerometer data [J]. *J. Geophys. Res.*, 2006, **111**: A06303

[14] EMMERT J T, PICONE J M, MEIER R R. Thermospheric global average density trends, 1967—2007, derived from orbits of 5000 near-Earth objects [J]. *Geophys. Res. Lett.*, 2008, **35**: L05101

[15] SOLOMON S C, QIAN L, DIDKOVSKY L V, *et al.* Causes of low thermospheric density during the 2007—2009 solar minimum [J]. *J. Geophys. Res.*, 2011, **116**: A00H07

[16] QIAN L, SOLOMON S C. Thermospheric density: an overview of temporal and spatial variations [J]. *Space Sci. Rev.*, 2012, **168**(1/2/3/4): 1-27

[17] JONES L M, PETERSON J W, SCHAEFER E J, *et al.* Upper-air density and temperature: some variations and an abrupt warming in the mesosphere [J]. *J. Geophys. Res.*, 1959, **64**(12): 2331-2340

[18] THIELE O W. Observed diurnal oscillations of pressure and density in the upper stratosphere and lower mesosphere [J]. *J. Atmos. Sci.*, 1966, **23**(4): 424-430

[19] YI W, XUE X, REID I M, *et al.* Climatology of the mesopause relative density using a global distribution of meteor radars [J]. *Atmos. Chem. Phys.*, 2019, **19**: 7567-7581

[20] RUSSELL J M, MLYNCZAK M G, GORDLEY L L. Overview of the Sounding of the Atmosphere Using Broadband Emission Radiometry (SABER) experiment for the Thermosphere-Ionosphere-Mesosphere Energetics and Dynamics (TIMED) mission [J]. *Opt. Photonics*, 1994. DOI: 10.1117/12.187579

[21] FECHINE J, WRASSE C M, TAKAHASHI H, *et al.* Lower-mesospheric inversion layers over Brazilian equatorial region using TIMED/SABER temperature profiles [J]. *Adv. Space Res.*, 2007, **41**(9): 1447-1453

[22] XIAO C, HU X, YANG J, *et al.* Characteristics of atmospheric density at 38°N in near space and its modeling technique [J]. *J. Beijing Univ. Aeronaut. Astronaut.*, 2017, **43**(9): 1757-1765

[23] HAUCHECORNE A, CHANIN M L. Density and temperature profiles obtained by lidar between 35 km and 70 km [J]. *Geophys. Res. Lett.*, 1980, **7**: 565-568

[24] SHIBATA T, KOBUCHI M, MAEDA M. Measurements of density and temperature profiles in the middle atmosphere with a XeF lidar [J]. *Appl. Optics*, 1986, **25**(5): 685-688

[25] DAO P, KLEMETTI W, SIPLER D, *et al.* Density measurements with combined Raman-Rayleigh lidar [J]. *Proc. SPIE Int. Soc. Opt. Eng.*, 1988, 1062: 138-143

[26] WU Y, HU H, HU S, *et al.* Atmospheric density and temperature measurement with lidar in the middle and upper stratosphere [J]. *Chin. J. Quant. Electron.*, 2000, **17**(5): 426-431

[27] BARTON D L, WICKWAR V B, HERRON J P, *et al.* Variations in mesospheric neutral densities from rayleigh lidar observations at Utah State University [C]//The 27th International Laser Radar Conference. New York: the International Laser Radar Conference, 2015

[28] QIAO S, PAN W, ZHU K, *et al.* Initial results of lidar measured middle atmosphere temperatures over Tibetan Plateau [J]. *Atmos. Oceanic Sci. Lett.*, 2014, **7**: 213-217

[29] QIAO S, PAN W, BAN C, *et al.* Mesospheric density measured by Rayleigh lidar over Golmud [J]. *Infrared Laser Eng.*, 2018, **47**(S1): S106005-1-6

[30] LOMB N R. Least-squares frequency analysis of unequally spaced data [J]. *Astrophys. Space Sci.*, 1976, **39**, 447-462

[31] PAN W, GARDNER C S. Seasonal variations of the atmospheric temperature structure at South Pole [J]. *J. Geophys. Res.*, 2003, **108**(D18): 4564